Available online at www.sciencedirect.com
SCIENCE DIRECT®
Journal of Sound and Vibration 287 (2005) 117–128
JOURNAL OF SOUND AND VIBRATION
www.elsevier.com/locate/jsvi

Lagging motion of forced nonlinear oscillators

Sarng Woo Karng[a], Ki Young Kim[b], Ho-Young Kwak[b,*]

[a]*Thermal/Flow Control Research Center, Korea Institute of Science and Technology, P.O. Box 131 Cheongryang, Seoul 130-650, Korea*
[b]*Mechanical Engineering Department, Chung-Ang University, 221, Huksuk-Dong, Dongjak-Ku, Seoul 156-756, Korea*

Received 12 January 2004; received in revised form 18 May 2004; accepted 27 October 2004
Available online 22 December 2004

Abstract

The lagging motion of nonlinear oscillators with respect to the externally driven field, which has never been discussed previously, was treated analytically and the calculation results were compared with the observed results. Such lagging motion may occur in nonlinear systems whose behavior crucially depends on the frequency of the applied force. The lagging motion of the nonlinear oscillator with respect to the harmonically driven field made the oscillator respond in a way that reduced the effect of the applied field. The calculation considering the lagging motion yielded proper results in the expansion ratio and trajectories in phase plane for the oscillating bubble under ultrasound and the frequency spectrum for a forced inverted pendulum.

1. Introduction

Forced oscillation of nonlinear oscillator has been studied extensively by many investigators because it possesses many interesting phenomena such as bifurcation, period doubling, strange attractor, and chaos [1,2]. It is well known that linear oscillators, such as harmonic oscillators, respond linearly to an external forcing field. However, the response of a nonlinear oscillator to the external forcing field is complex and hard to be analyzed.

Recently, it was found that a bubble, which is a typical nonlinear oscillator driven by ultrasound, responded quite differently from what we predicted by a conventional method. In

*Corresponding author. Tel.: +82 2 820 5278; fax: +82 2 826 7464.
E-mail address: kwakhy@cau.ac.kr (H.-Y. Kwak).

0022-460X/$ - see front matter © 2004 Elsevier Ltd. All rights reserved.
doi:10.1016/j.jsv.2004.10.034

fact, the maximum radius and the expansion ratio R_{max}/R_0 (maximum radius divided by equilibrium radius) obtained from an air bubble at a driving frequency of 12.926 kHz and driving amplitude of 1.33 atm at a water temperature of 23.5 °C were considerably less than the predicted values by the Rayleigh–Plesset equation or the Keller–Miksis equation with a conventional numerical technique [3]. Also, the calculated frequency spectrum of the inverted pendulum by the conventional method is quite different from the frequency spectrum observed.

In this study, the lagging motion of nonlinear oscillator to the externally driven field was treated analytically and the calculation results were compared with the observed results. Lagging motion between the nonlinear oscillator and the harmonically driven field was found in this study. Such lagging, in turn, made the nonlinear oscillator respond in a way that reduced the effect of the applied force so that this phenomenon may be considered as the ''Le Châtelier's principle'' [4] in nonlinear systems.

2. Bubble motion under ultrasound

For the bubble wall motion, the Rayleigh–Plesset equation [RP] using the assumption of the polytropic behavior for gas inside the bubble and the Keller–Miksis equation using the analytical solutions of the Navier–Stokes equations [KMNS] yielded the same bubble radius–time curve except near the collapse point and the subsequent bouncing motion even though the gas temperature and pressure predicted by the two methods were quite different [5]. Consider the problem that occurred during the integration of the bubble wall motion under driving frequency f_d, which is different from the natural frequency of bubble motion $1/t_0$, defined later in Eq. (5b), with the simple Rayleigh–Plesset equation.

2.1. Rayleigh–Plesset [RP] equation

The modified RP equation [6], taking account of the compressible behavior of liquid is given by

$$\rho_\infty\left(R_b\ddot{R}_b+\frac{3}{2}\dot{R}_b^2\right)=\left(1+\frac{R_b}{C_\infty}\frac{\mathrm{d}}{\mathrm{d}t}\right)(P_b-P_\infty-P_s(t))-4\mu_l\frac{\dot{R}_b}{R_b}-\frac{2\sigma}{R_b}, \tag{1}$$

where R_b is the instantaneous bubble radius, C_∞ is the sound speed in the liquid, ρ_∞ is the density of medium, P_∞ is the ambient pressure and σ and μ are the surface tension and dynamic viscosity of liquid, respectively. The pressure of the driving sound P_s may be represented by a sinusoidal function such as

$$P_s(t)=-P_A\sin\omega_d t, \tag{2}$$

where P_A is the amplitude of the ultrasound, $\omega_d=2\pi f_d$ and f_d is the frequency of the driving ultrasound. For the calculation of the gas pressure inside the bubble, Hilgenfeldt et al. [7] employed the following van der Waals equation with a polytropic exponent of Γ.

$$P_b=\left(P_\infty+\frac{2\sigma}{R_b}\right)\left(\frac{R_0^3-h^3}{R_b^3-h^3}\right)^\Gamma, \tag{3}$$

where $h = R_0/8.5$ is the hard core van der Waals' radius for air, R_0 is an equilibrium radius, and the polytropic index Γ is taken to be unity. Certainly, Eq. (3) which assumes the isothermal and uniform behavior of the gas inside the bubble is not adequate to estimate the gas temperature inside the bubble around the collapse point [8]. The isothermal behavior of the gas inside bubble was valid only in the expansion phase up to the maximum radius [6,9]. To calculate the temperature, they employed the following relation using the variable polytropic index of γ_p which is related to the Péclet number at the bubble wall.

$$\frac{T_b}{T_\infty} = \left(\frac{R_0^3 - h^3}{R_b^3 - h^3}\right)^{\gamma_p - 1}. \tag{4}$$

The polytropic index of γ_p, which depends on the bubble radius R_b, wall velocity $\dot{R}_b$ and the gas temperature T_b, has maximum value about 1.6. With this value of γ_p, one may estimate the gas temperature at the collapse point from Eq. (4).

2.2. A procedure of integration for the RP equation

Eq. (1) may not be integrated numerically properly without normalization of the physical variables by using the corresponding characteristic quantities. These quantities which are naturally chosen characterize the bubble motion. For instance, normalization of the governing equations may be done as follows [9]. The radius is compared to the equilibrium radius R_0, and the temperature and pressure are related to the ambient properties T_∞ and P_∞, respectively. Other characteristic quantities may be chosen as follows:

$$\text{Velocity:} \quad u_0 = \sqrt{P_\infty/\rho_\infty}, \tag{5a}$$

$$\text{Time:} \quad t_0 = R_0/u_0 = R_0/\sqrt{P_\infty/\rho_\infty}, \tag{5b}$$

$$\text{Dynamic viscosity:} \quad \mu_0 = P_\infty R_0/u_0, \tag{5c}$$

and

$$\text{Surface tension:} \quad \sigma_0 = P_\infty R_0. \tag{5d}$$

After the normalization procedure, the Rayleigh–Plesset equation using the nondimensional variables except the variables in the cosine function such as f_d and t becomes

$$\left(R\ddot{R} + \frac{3}{2}\dot{R}^2\right) = \left(1 + \frac{R}{C_\infty}\frac{\mathrm{d}}{\mathrm{d}t}\right)(P_b - 1 + P_A\cos[2\pi f_d t]) - 4\mu_l\frac{\dot{R}}{R} - \frac{2\sigma}{R}. \tag{6}$$

Usually the time t and the driving frequency f_d in the sinusoidal term in Eq. (6) were normalized by t_0 and $1/t_0$, respectively [10,11] so that the nondimensional form of the sinusoidal term becomes $\cos(2\pi f t)$ where $f = f_d t_0$ is the nondimensional frequency which is quite different from the original driving frequency. Also, the bubble motion described by Eq. (6) is normalized by t_0 for time scale so that the calculated nondimensional time for bubble motion can be recovered by t_0 (single time normalization method). However, such single time normalization results in moving in phase with the driving ultrasound or moving under different driving frequency, which might cause "artificial resonance". It is also noted that the expansion ratio [10] and consequently the gas temperature and

pressure and the bubble wall velocity at the collapse point increase considerably by the reduction in the nondimensional frequency $f_d t_0$ with such normalization method.

The artificial resonance effect due to improper choice of the characteristic frequency of the driving ultrasound during numerical evaluation for the bubble wall motion can be avoided. Another normalization method to avoid the artificial resonance is as follows. In general, the characteristic frequency of the driving force f_0 to be chosen differs from the natural frequency of bubble oscillation $1/t_0$. The time t and the driving frequency f_d in the sinusoidal term in Eq. (6) are normalized by $1/f_0$ and f_0, respectively so that the sinusoidal term remains as the same form as $\cos(2\pi ft)$ but with different nondimensional frequency $f = f_d/f_0$. Because the bubble wall motion described by Eq. (6) is also normalized by t_0 with this normalization method but the nondimensional time is recovered by $1/f_0$ in numerical procedure (two time normalization method), there is a lagging time of the bubble motion with respect to the characteristic time of the applied ultrasound f_0, which is defined as [5]

$$\tau = 1/f_0 - t_0. \tag{7}$$

Eq. (7) gave reasonable results when one took τ as comparable value of t_0. Eq. (7) means that the bubble motion is characterized by the time scale of $t_0 + \tau$, having lagging time of τ with respect to the characteristic time scale of applied field, $1/f_0$.

A physical basis of the lagging motion for the bubble behavior under ultrasound may be described as follows. It is well known that the bubble will be viscoelastic if the bubble is deformable, even if the gas inside and the surrounding liquid are both Newtonian [12]. The characteristic time which represents the retarded mechanical response [13] of the bubble may be defined as [12]

$$\tau_c = \frac{R_b \mu}{\sigma}. \tag{8}$$

For the gas bubble with an equilibrium radius of 5 μm in water, the characteristic time is about 0.1 μs, which is close to the value obtained from Eq. (7). Neither the surface tension nor the viscosity value of water only affects the motion of the bubble of micrometer size very much. However, the combined effect of the surface tension and the viscosity enhances the stability of the sonoluminescing gas bubble significantly, which shows a subtle nature of bubble motion in ultrasound.

2.3. Keller–Miksis formulation with the analytical solution for the Navier–Stokes equation

For bubble wall motion, the equation from Keller and Miksis formulation [14] and the analytical solutions for the Navier–Stokes equations for the gases inside bubble (KMNS) [15] in spherical symmetry may be utilized. The Keller–Miksis equation which accounts for the effects of liquid compressibility is as follows:

$$R_b\left(1 - \frac{U_b}{C_b}\right)\frac{\mathrm{d}U_b}{\mathrm{d}t} + \frac{3}{2}U_b^2\left(1 - \frac{U_b}{3C_b}\right) = \frac{1}{\rho_\infty}\left(1 + \frac{U_b}{C_b} + \frac{R_b}{C_b}\frac{\mathrm{d}}{\mathrm{d}t}\right)\left[P_B - P_s\left(t + \frac{R_b}{C_b}\right) - P_\infty\right], \tag{9}$$

where U_b is the speed of the bubble wall, C_b is the sound speed of liquid at the bubble wall, and liquid pressure on the external side of the bubble wall P_B is related to the pressure inside the

bubble wall P_b by $P_B = P_b - 2\sigma/R_b - 4\mu U_b/R_b$. The above equation based on acoustical assumption is valid as long as the bubble wall velocity is less than the sound speed at the bubble wall C_b. In the KMNS formulation, the time-dependent pressure and temperature at the bubble center may be obtained by solving the mass, momentum, and energy equation for the gas inside bubble [16]. Also the heat transfer through the bubble wall was considered by solving the mass and energy equation for the liquid adjacent to the bubble wall [17]. Eq. (9) can be normalized using the same method discussed in previous section.

The two time normalization method introduced above gives a physical approximation which represents the lagging behavior of bubble motion (a nonlinear oscillator) under ultrasound. Such lagging may occur in the other nonlinear oscillator systems such as an inverted pendulum, which will be discussed next.

3. Forcing motion of inverted pendulum

Consider a damped, harmonically driven, inverted pendulum which was analyzed and tested by Beckert et al. [18] and was also tested experimentally by Chancellor et al. [19]. Detailed discussion on the experimental set up for an inverted pendulum is in Chancellor et al. [19]. The equation of motion for the inverted pendulum tested is given by

$$I_0\ddot{\theta} + C_t\dot{\theta} + K_t\theta - M_0 g R_d \sin\theta = K_t\theta_0 \sin[\Omega_d t], \tag{10}$$

where I_0 is the disk mass moment of inertia, C_t is the damping coefficient, K_t is the torsional spring constants, M_0 is the disk added mass, R_d is the disk radius, and θ_0 is the angular displacement excitation of the inverted acceleration. In Eq. (10), Ω_d denotes the driving frequency on the inverted pendulum and g is the gravitational constant. The actual physical parameters measured from the experimental apparatus are shown in Table 1.

Nondimensionalizing Eq. (10) with respect to t_P, the characteristic time scale of the inverted pendulum, we can write Eq. (10) as

$$\frac{\mathrm{d}^2\theta}{\mathrm{d}t^{*2}} + \frac{C_t t_P}{I_0}\frac{\mathrm{d}\theta}{\mathrm{d}t^*} + \frac{K_t t_P^2}{I_0}\theta - \frac{M_0 g R_d t_P^2}{I_0}\sin\theta = \frac{K_t t_P^2 \theta_0}{I_0}\sin[\Omega_d t_P t^*]. \tag{11}$$

Choosing the natural frequency of the inverted pendulum Ω_P as

$$\Omega_P = \frac{1}{t_P} = \sqrt{K_t/I_0}. \tag{12}$$

Table 1
Measured parameter values for inverted pendulum [19]

Disk moment of inertia, I_0	0.00147 kg m^2
Torsional spring constant, K_t	0.0183 N m/rad
Added mass, M_0	0.0267 kg
Disk radius, R_0	0.0845 m
Angular displacement excitation, θ_0	0.094 rad
Driving frequency range	0.1–1.0 Hz

Eq. (10) with a value of $C_t/I_0 = 0.45$ and an angular excitation value $\theta_0 = 0.094$, becomes

$$\frac{d^2\theta}{dt^{*2}} + 0.1275\frac{d\theta}{dt^*} + \theta - 1.208\sin\theta = 0.094\sin[\Omega_d t_P t^*]. \tag{13}$$

This inverted pendulum which showed chaotic response at $C_t/I_0 = 0.45$ created two stable fixed points at approximately $\pm 60^\circ$ from the vertical with an added mass of 0.0267 kg [19].

If the driving frequency Ω_d in the sinusoidal term in Eq. (13) is normalized by the natural frequency of the inverted pendulum $\Omega_P = 1/t_P$, the sinusoidal term becomes $\sin(\Omega_d^* t^*)$ where $\Omega_d^* = \Omega_d/\Omega_P$ is the nondimensional forcing frequency (single time normalization method). However, if we nondimensionalize the driving frequency and the time in the sinusoidal term in Eq. (13) as another characteristic forcing frequency $\Omega(\neq\Omega_P)$ and the corresponding time scale $1/\Omega$ (two time normalization method) respectively, the lagging time between the oscillator motion and the applied force would be generated, such as

$$\tau_P = \frac{1}{\Omega} - t_P \tag{14}$$

so that the sine term in Eq. (13) becomes $\sin[\Omega_d^* t^*]$ where $\Omega_d^* = \Omega_d/\Omega$.

4. Calculation results and discussion

The calculation results obtained by using the two kinds of normalization methods of the governing equation for the bubble motion described were presented and compared with the observed results. As shown in Fig. 1, the expansion ratio calculated by the Rayleigh–Plesset equation without considering the lagging time or $\tau = 0$ is as much as 17.2 at the ultrasound amplitude of 1.33 atm and driving frequency of 12.926 kHz. Almost the same results is obtained by the KMNS method with zero lagging time. On the other hand the expansion ratio calculated by KMNS method for the bubble of an equilibrium radius of 5 μm under the same amplitude and frequency of ultrasound becomes as small as 9.76 with the lagging time of 0.39 μs. Similar results can be obtained using RP with a lagging time of 0.39 μs. As shown in Fig. 1, the result obtained with the finite lagging time agrees well with the observed results obtained by CCD camera with a microscope [3]. For the oscillating bubble of $R_0 = 5.0\,\mu m$ in the medium of ρ_∞ and P_∞, the characteristic frequency of the bubble motion $1/t_0$ is about 2.0×10^6/s while the characteristic frequency of the applied ultrasound f_0 is about 1.124×10^6/s if lagging time of 0.39 μs is used. The observed results confirm that the bubble does not move in phase with the applied ultrasound so that the measured expansion ratio is about 9.76. Certainly one cannot obtain this observed value of the expansion ratio with the single time normalization method or no lagging time ($\tau = 0$) of the bubble motion with respect to the driving ultrasound.

In Fig. 2, the observed and calculated trajectories in phase plane for an air bubble of $R_0 = 1.3\,\mu m$ at $P_A = 1.12$ atm and $f_d = 28.84$ kHz are shown. In the observed trajectories [20] shown in Fig. 2a, there are several inner loops showing a period-three oscillation. However, the calculated trajectory by RP with no lagging time shows just a period-one oscillation as can be seen in Fig. 2b. This trajectory is quite different from the trajectory obtained by RP with a lagging time $\tau = 2.64\,\mu s$ as shown in Fig. 2c. Fig. 2c shows similar period-three oscillation as observed although the

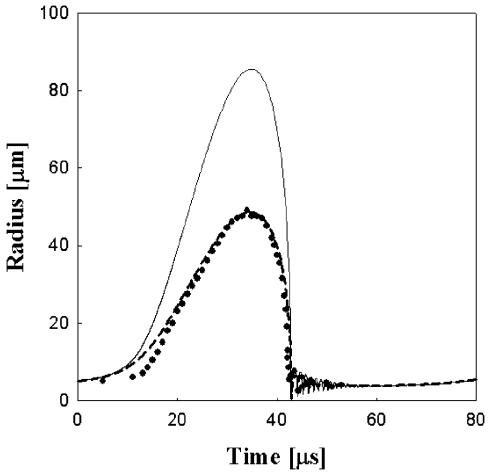

Fig. 1. Radius versus time for one cycle of an air bubble oscillations at $P_A = 1.33$ atm, $f_d = 12.926$ kHz and water temperature of 23.5 °C. The equilibrium radius of the air bubble was estimated to be about 5.0 μm. Full circles indicate the data obtained by CCD camera with a microscope [3], full line for the calculation results by RP and KMNS without lagging time ($\tau = 0$), and dotted line for the calculation results by KMNS with $\tau = 0.39$ μs.

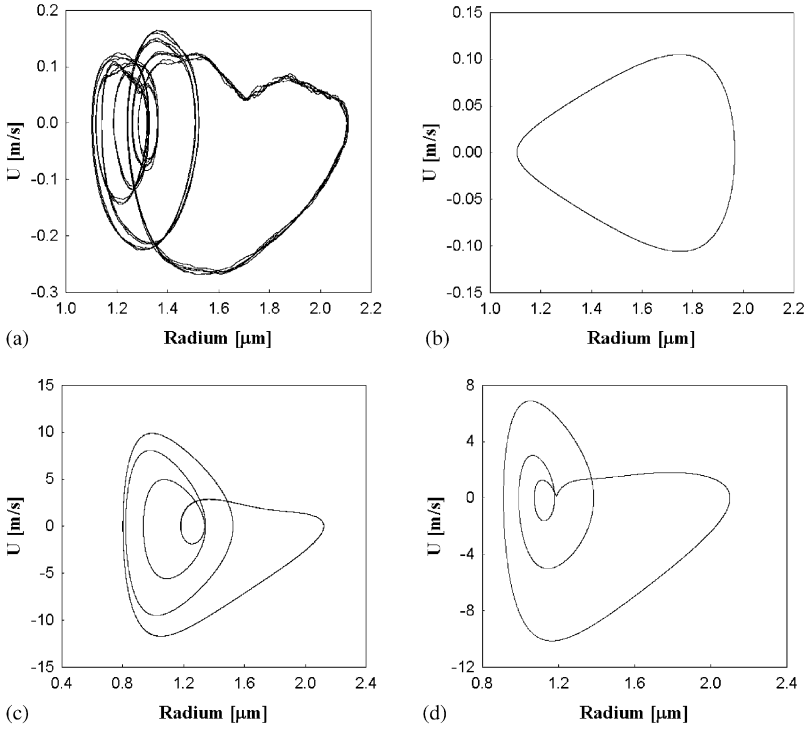

Fig. 2. Trajectories in phase space for an air bubble oscillation for $R_0 = 1.3$ μm at $P_A = 1.12$ atm and $f_d = 28.84$ kHz: (a) observed results by light scattering method [20], (b) calculation results by RP without lagging time, (c) calculation results by RP with $\tau = 2.64$ μs, (d) calculation results by KMNS with $\tau = 2.64$ μs.

calculated values of the maximum and minimum velocities in the phase plane trajectory were quite different from the observed one. Such large values in velocities happen because the RP equation with the polytropic index does not account for thermal damping due to the finite heat transfer through the bubble wall. On the other hand, the KMNS method which included the heat transfer adjacent the bubble wall yielded proper trajectory and much less velocity values in phase plane, as shown in Fig. 2d.

The fact that a proper lagging time is needed to describe the bubble behavior even for smaller equilibrium radius may be confirmed convincingly by inspecting the case of $R_0 = 0.8\,\mu m$ at $P_A = 1.10\,atm$, shown in Fig. 3a, which shows only two bouncing motion after the first minimum. Similiar behavior of bubble as the observed one may be obtained with the relaxation time of 4.08 μs either by KMNS or by RP, which is quite larger relaxation time than those employed in previous examples as can be seen in Fig. 3b.

The lagging discussed on the bubble behavior under ultrasound may happen in another nonlinear system. Let us consider the calculated and observed results obtained from the inverted pendulum discussed previously. A phase portrait for the inverted pendulum at a forcing frequency 1.5 rad/s and an amplitude 0.094 rad with the single time normalization method is shown in Fig. 4a. The corresponding Poincaré map obtained at a phase of 60° is shown in Fig. 4b. The results shown in Fig. 4 were the last 100 cycles obtained by analyzing a sequence of 1000 cycles with the value $C_t/I_0 = 0.45$ where chaotic response occurred in the experiment [19]. As shown in Fig. 4a, any phase trajectory does not coincide with the other trajectories, which show typical chaos regime. In the Poincaré section shown in Fig. 4b, a double line structure like that found in strange attractors [1] can be seen. The trajectories and the Poincaré map in Fig. 4 show similar results for a two-well potential [21,22]. As expected, the maximum and minimum angular velocities were obtained at angular positions of 1 and −1 rad, respectively. However, the calculated maximum and minimum angular velocities were 20% larger than the absolute value of the observed velocities. Further, the calculated frequency spectrum of the inverted pendulum at the input of a single frequency sinusoidal excitation shows a continuous spectrum of frequencies below the single characteristic frequency with the single time normalization method, as can be

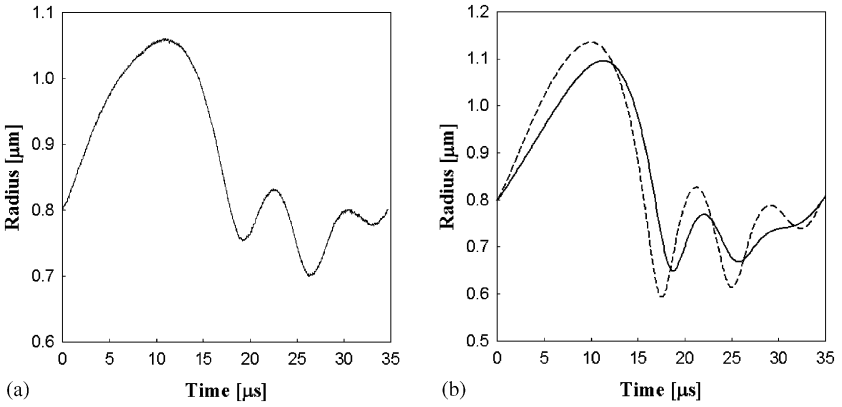

Fig. 3. Radius–time curve for air bubble of $R_0 = 0.8\,\mu m$ at $P_A = 1.10\,atm$ and $f = 28.84\,kHz$: (a) observed data by light scattering method [20], (b) calculated one by KMNS with relaxation time of 4.08 μs (—) and by RP with relaxation time of 4.08 μs (- - -).

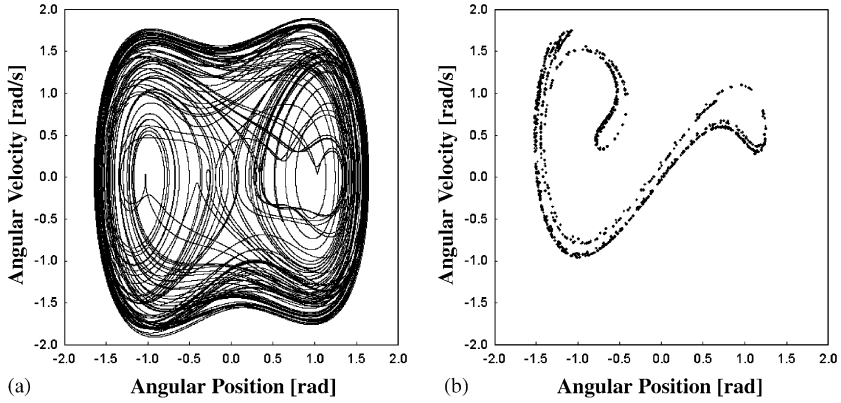

Fig. 4. Trajectories in phase space (a) and Poincaré map (b) for inverted pendulum at forcing frequency 1.5 rad/s and amplitude 0.094 rad with no lagging time.

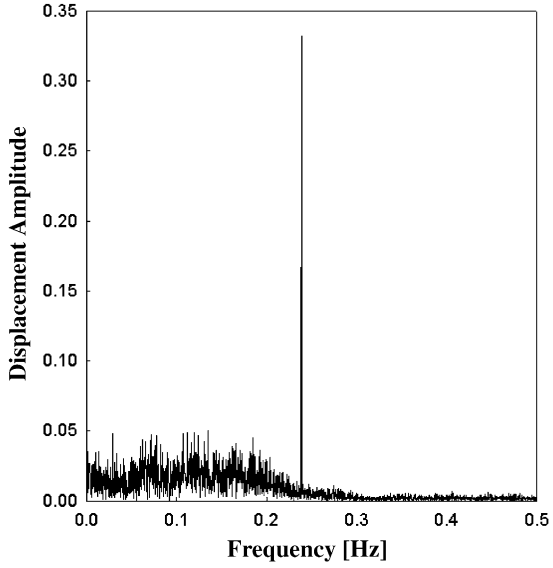

Fig. 5. Frequency spectrum of the response of inverted pendulum at forcing frequency 1.5 rad/s and amplitude 0.094 rad with no lagging time.

seen in Fig. 5. Although this calculation result with the single time normalization method shows one of the characteristics of chaotic vibrations, the calculated spectrum is quite different from the frequency spectrum of the response observed in the experiment [19].

One can obtain quite different results, as shown in Fig. 6, when one uses the two time normalization method with a relaxation time $\tau_p = 0.046$ s. As shown in Fig. 6a, the trajectories in phase plane become more ordered and are confined to a well-defined layer of phase space. The corresponding Poincaré map shown in Fig. 6b tends to be localized into several regions. Both the

Poincaré map in Fig. 6b and the trajectories in phase space in Fig. 6a suggest that a periodic subharmonic orbit exists. Further the broad-band spectrum disappears to noise levels, and a $\frac{1}{3}$ subharmonic and a $\frac{5}{3}$ harmonic in the frequency spectrum appear instead so that this spectrum is very similar to the spectrum calculated from the observed angular velocity data depending on angular position [19]. In fact, the Poincaré map and the frequency spectrum obtained with the two time normalization method may be considered as a precursor to the fully developed chaos obtained with single time normalization as shown Figs. 4 and 5. Correct value of lagging time may be determined by the characteristics of nonlinear systems. Therefore, lagging of the nonlinear oscillator with respect to the sinusoidally driven field makes the oscillator respond in a way that

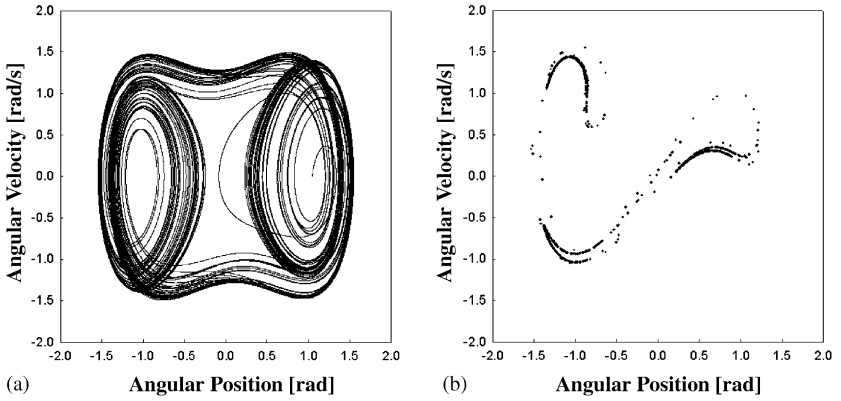

Fig. 6. Trajectories in phase space (a) and Poincaré map (b) for inverted pendulum at forcing frequency 1.5 rad/s and amplitude 0.094 rad with lagging time $\tau_P = 0.046$ s.

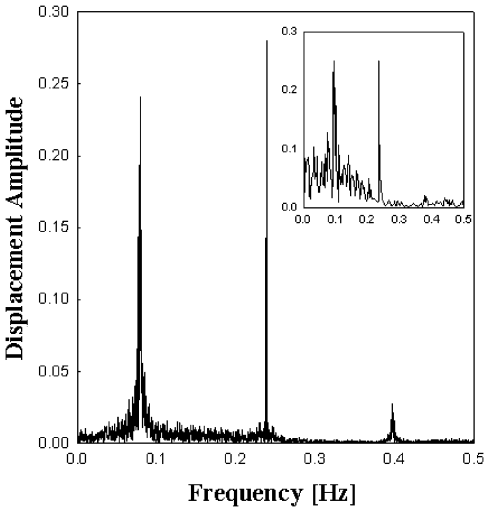

Fig. 7. Calculated and observed (inset) [19] frequency spectrum of the response of inverted pendulum at forcing frequency 1.5 rad/s and amplitude 0.094 rad with lagging time $\tau_P = 0.046$ s.

reduces the effect of the applied force, which may be explained as the Le Châtelier's principle in broad sense (Fig. 7).

5. Conclusion

Forced oscillation of nonlinear oscillations such as oscillation of a single bubble under ultrasound and motion of an inverted pendulum under harmonically driven force was studied analytically. The calculation results with an assumption that the nonlinear oscillator moves in phase with the harmonically driven field overpredicted the amplitude of response. However, the calculation considering the lagging motion of the nonlinear oscillator with respect to the applied field yielded proper results for the expansion ratio and the trajectories in phase plane for the bubble under ultrasound, and frequency spectrum of the response for the forced inverted pendulum.

Acknowledgements

This work has been supported by the grants from Korea Science and Engineering Foundation under Contract 1999-1-304-002-5.

References

[1] F.C. Moon, *Chaotic and Fractal Dynamics*, Wiley, New York, 1992.
[2] S.H. Strogatz, *Nonlinear Dynamics and Choas*, Addison-Wesley, Reading, MA, 1994.
[3] J. Jeon, J. Lee, H. Kwak, Possibility of upscaling for single bubble sonoluminescence at a low driving frequency, *Journal of the Physical Society of Japan* 72 (2003) 509–515.
[4] H.B. Callen, *Thermodynamics and an Introduction to Thermostatistics*, second ed., Wiley, New York, 1985.
[5] H. Kwak, J. Lee, S. Karng, Bubble dynamics for single bubble sonoluminescence, *Journal of the Physical Society of Japan* 70 (2001) 2909–2917.
[6] R. Löfstedt, B.P. Barber, S.J. Putterman, Toward a hydrodynamic theory of sonoluminescence, *Physics of Fluids A* 5 (1993) 2911–2928.
[7] S. Hilgenfeldt, D. Lohse, M.P. Brenner, Phase diagram for sonoluminescing bubbles, *Physics of Fluids* 8 (1996) 2806–2808.
[8] S. Putterman, P.G. Evans, G. Vasquez, K. Weninger, Is there a simple theory of sonoluminescence?, *Nature* 409 (2001) 782–783.
[9] H. Kwak, H. Yang, An aspect of sonoluminescence from hydrodynamics theory, *Journal of the Physical Society of Japan* 64 (1995) 1980–1992.
[10] S. Hilgenfeldt, D. Lohse, Predictions for upscaling sonoluminescence, *Physical Review Letters* 82 (1999) 1036–1039.
[11] A. Prosperetti, Y. Hao, Modeling of spherical gas bubble oscillations and sonoluminescence, *Philosophical Transactions of the Royal Society of London Series A* 357 (1999) 223–230.
[12] R.G. Larson, *The Structure and Rheology of Complex Fluids*, Oxford University Press, New York, 1999.
[13] G. Strobl, *The Physics of Polymers*, Springer, Berlin, 1997.
[14] J.B. Keller, M. Miksis, Bubble oscillations of large amplitude, *Journal of the Acoustical Society of America* 68 (1980) 628–633.

[15] H. Kwak, J. Na, Hydrodynamic solutions for a sonoluminescing gas bubble, *Physical Review Letters* 77 (1996) 4454–4457.
[16] H. Kwak, J. Na, Physical processes for single bubble sonoluminescence, *Journal of the Physical Society of Japan* 66 (1997) 3074–3083.
[17] J.C. Ryu, H. Kwak, Bifurcation phenomena for the damped bubble oscillation in periodically driven pressure fields, in: H.H. Bau, L.A. Bertram, S.A. Korpela (Eds.), *Bifurcation Phenomena and Chaos in Thermal Convection, HTD-214*, ASME, New York, 1992, pp. 1–8.
[18] S. Beckert, U. Schock, C.-D. Schulz, T. Weidlich, F. Kaiser, Experiments on the bifurcation behavior of a forced nonlinear pendulum, *Physics Letters A* 107 (1985) 347–350.
[19] R.S. Chancellor, R.M. Alexander, S.T. Noah, Detecting parameter ranges using experimental nonlinear dynamics and chaos, *Journal of Vibration and Acoustics* 118 (1996) 375–383.
[20] B. Kim, J. Jeon, H. Kwak, Stability and selective bifurcation for a gas bubble oscillating under ultrasound, *Journal of the Physical Society of Japan* 68 (1999) 1197–1204.
[21] J. Guckenheimer, P. Holmes, *Nonlinear Oscillations, Dynamical Systems, and Bifurcations of Vector Fields*, Springer, Berlin, 1983.
[22] J. Awrejcewicz, *Bifurcation and Chaos in Coupled Oscillators*, World Scientific, Singapore, 1991.